Energy and Built Environment 1 (2020) 242–253

Contents lists available at ScienceDirect

Energy and Built Environment

journal homepage: www.elsevier.com/locate/enbenv

Effect of traffic tidal flow on pollutant dispersion in various street canyons and corresponding mitigation strategies

Zhengtong Li[a], Tianhao Shi[b], Yongjia Wu[b], Hao Zhang[a], Yu-Hsuan Juan[c], Tingzhen Ming[b,d,*], Nan Zhou[d]

[a] Department of Mechanical Engineering, The Hong Kong Polytechnic University, Kowloon, Hong Kong SAR, China
[b] School of Civil Engineering and Architecture, Wuhan University of Technology, Wuhan, China
[c] Department of the Built Environment, Eindhoven University of Technology, Eindhoven, the Netherlands
[d] China Energy Group, Environmental Energy Technologies Division, Lawrence Berkeley National Laboratory, 1 Cyclotron Road, Berkeley, CA 94720, USA

ARTICLE INFO

Keywords:
Street canyon
Intake fraction
Computational fluid dynamics (CFD)
Wind catchers

ABSTRACT

Increasing traffic emission presents a high risk of exposure to residents in near-road buildings. Traffic tidal flow (TTF) has gradually become one of the most important components of urban traffic congestion. By computational fluid dynamics simulation, the present study examines the airflow, spatial distribution of pollutant concentration, and personal intake fraction (*IF_p*) of CO in five street canyon structures (shallow, regular, deep, step-up, and step-down street canyons), with non-uniform TTF-induced traffic emission considered. Optimal urban design devices (wind catchers) are subsequently introduced to reduce *IF_p*.

The results suggest that leeward *IF_p* is far higher in concentration than the windward wall in the shallow, regular, step-up, and step-down street canyons but lower than the windward side in the deep street canyon under different TTF conditions. Moreover, the TTF condition S_L (leeward source)/S_W (windward source)=3/1 leads to a higher leeward *IF_p* in the shallow, regular, deep, and step-up street canyons, compared with S_L/S_W=1/3; however, no significant difference in windward *IF_p* is found under the different TTF conditions. The highest *IF_p* and lowest *IF_p* for both TTF configurations occur in the step-down and shallow street canyons, respectively. Finally, the effect of wind catchers (WCs) varies between the street canyon structures under different TTF conditions. WCs can lead to at least 30.6% reduction in leeward overall average *IF_p* (<*IF_p*>) in the shallow, regular, step-up, and step-down street canyons, as well as 12.8%–78.4% decrease in windward ⟨*IF_p*⟩ owing to the WCs in the regular, deep, step-up, and step-down street canyons.

1. Introduction

Driven by rapid economic development and urbanization, the rural population has been flocking to the big cities. While cities with developed industry and commerce and perfect infrastructure have provided convenience to people, they have also encountered serious environmental problems. [1]. Simultaneously, high-density urban buildings increase the number of residences but reduce the ventilation capacity of the city. This occurrence hinders the rapid dilution and dispersion of pollutants emitted by vehicles, aggravating air pollution [2]. To address and further reduce severe pollution, considerable research has been conducted [3–16]. The majority of these studies report on identical pollutant sources on different sides [4,17–20]. Traffic emission from different sides can entirely vary, particularly when traffic tidal flow (TTF) occurs. TTF, which is characterized by a very heavy traffic flow on one side and an unobstructed traffic flow on the other side during rush hours, occurs when the commercial and residential areas are separated by urban development [21]. Recently, TTF has gradually become one of the most important components of urban traffic congestion during peak commute periods in large- and medium-sized cities in China (Fig. 1). Thus, basic scientific understanding of the distinct transport of airborne pollutants within urban areas where TTF occurs is needed.

Street canyons vary in structure, including the aspect ratio (*AR*) [22–26], asymmetry [27,28], and so on, which significantly influence wind field and pollutant dispersion within the street canyons. *AR* is defined as the building height-to-street width ratio (*H*/*W*, where *H* is the building height, and *W* is the street width). Variations in *AR* can lead to different flow patterns and capacities of pollution diffusion within street canyons [29–33]. Liu et al. [34] found that ventilation was enhanced with a reduction in *H*/*W*, but the maximum pollutant removal was at *H*/*W* = 0.8. Murena and Vorraro [35] determined by field measurement that pollutant concentration in a deep canyon (*H*/*W* = 5.7) was

* Corresponding author.
E-mail address: tzming@whut.edu.cn (T. Ming).

https://doi.org/10.1016/j.enbenv.2020.02.002
Received 8 September 2019; Received in revised form 21 November 2019; Accepted 22 February 2020
Available online 6 March 2020

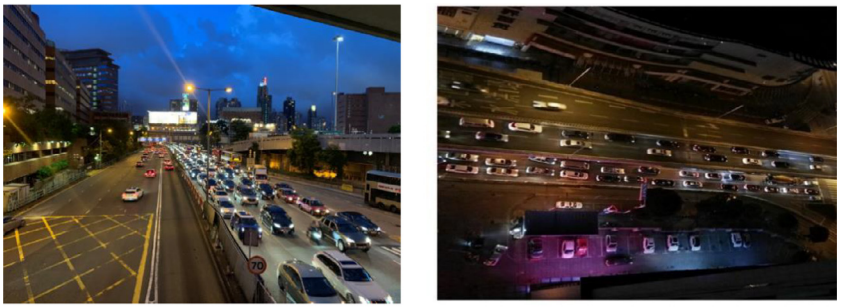

Hong Kong, China WuHan, China

Fig. 1. Photos showing traffic tidal flow in a realistic urban area.

three times that in a regular canyon ($H/W = 1$). With an increase in *AR*, pollution diffusion capacity and air quality within street canyons were reduced [36]. Moreover, Gu et al. [3] emphasized the effect of asymmetry on flow patterns and turbulence. Simulation of uniform street canyons may produce airflow patterns and spatial distribution of pollutants totally different from those of non-uniform street canyons. Using laboratory-scale experiments, Baik and Park [37] identified the creation of different vortices in various asymmetric street canyons. On the basis of these experiments, one vortex was observed within a step-up street canyon, but two counter-rotating vortices were observed in the canyon with a step-down notch. In the study by Nelson et al. [38], conducted field measurements of the wind field within the Oklahoma City Park Avenue street canyon showed that the non-uniform building arrangements could lead to a wind downdraft and horizontal divergence. To the best of our knowledge, the peculiarity of the little existing research on symmetric and asymmetric aspect ratios exists, but the analysis of its effect on the spatial distribution of pollutant concentration when TTF occurs is rarely reported.

Apart from the understanding of the spatial distribution of pollution, optimal techniques in urban design should be explored to maintain good ventilation and reduce high risk to pollutant exposure resulting from TTF. Setting wind catchers (WCs) is an effective method to enhance ventilation in street canyons by introducing fresh ambient wind from an upper level. Chew et al. [39] explored the potential of a WC to enhance air quality by installing a WC prototype in a water channel. Experiments showed that a WC enhances pedestrian-level wind speed in the target canyon by 2.5 times. Similarly, Zhang et al. [40] evaluated the effect of setting WCs on reducing vehicle pollution in deep canyon streets via CFD simulation. Consequently, the wind speed in the upper regions of the street canyon is considerably increased, particularly for wind in and below the WCs. In addition, normalized velocities at the pedestrian level are significantly increased owing to WCs, thereby reducing the CO concentration by one or two orders of magnitude. In the present study, we introduce the WC to explore how it can improve the dispersion of pollutants under TTF conditions.

To elucidate the influence of the street canyon structure on pollutant dispersion when TTF occurs, this study conducts CFD simulations to evaluate the effects of symmetric and asymmetric aspect ratios (*ARs* and *AARs*) on the spatial distribution of pollutant concentrations under various TTF conditions. Moreover, the potential of optimal technique in urban design (WC) on the mitigation of airborne pollutant induced by TTF is explored by comparing the difference in air quality index with or without WCs.

2. Methodology

2.1. Experimental data for CFD validation

The numerical accuracy of current CFD models was evaluated using wind data by Brown et al. A total of 77 cubes with 7-row and 11-column buildings arranged under an approaching wind parallel to the main streets (Fig. 2(a)) were investigated, where *x*, *y*, and *z* denote the streamwise, lateral, and vertical axes. In the wind-tunnel experiment, all characteristic dimensions of the three-dimensional (3D) building array—that is, the building width (*B*), building height (*H*), and street width (*W*)—are equal to 0.15 m. In Fig. 2(a), $x/H = 0$ represents the location of the upstream edge of the first row of cubes, and $y/H = 0$ denotes the vertical symmetric plane of the middle column. A neutral atmospheric boundary layer was formed, with a depth of 1.8 m, a power law exponent of 0.16, and a friction velocity u^* of 0.24 m/s, which could be expressed in the power-law form.

2.2. Computational approaches

2.2.1. Governing equation

A theoretical model built using ANSYS/Fluent® CFD software 15.0 was used to simulate the neutrally stratified atmospheric boundary layer over an array of 3D buildings under TTF conditions. The steady-state incompressible isothermal flow field and turbulent quantities were solved using the following governing equations:

$$\frac{\partial u_i}{\partial x_i} = 0 \tag{1}$$

$$\frac{\partial u_i \partial u_j}{\partial x_j} = -\frac{1}{\rho}\left(\frac{\partial p}{\partial x_i}\right) + g_i + \frac{\partial}{\partial x_j}\left[(\nu + \nu_t)\left(\frac{\partial u_i}{\partial x_j} + \frac{\partial u_j}{\partial x_i}\right)\right] \tag{2}$$

where u_i represents the velocity component in the i direction, and p, ρ, υ, υ_t, and g_i denote the pressure, density, laminar kinematic viscosity, turbulent kinematic viscosity, and acceleration of gravity, respectively.

In addition, the species transport equation was solved to probe the pollutant dispersion in an urban environment, as follows:

$$\frac{\partial u_i Y}{\partial x_i} - \frac{\partial}{\partial x_i}\left[(D + D_t)\frac{\partial Y}{\partial x_i}\right] = S \tag{3}$$

where D represents the molecular diffusion coefficient; $D_t (= \nu_t / S_{ct})$ denotes the turbulent diffusion coefficient of the pollutants, with ν_t as the turbulent viscosity, and S_{ct} as the turbulent Schmidt number equal to 0.4 to consider the underestimation of the turbulent mass diffusion from the Reynolds-averaged Navier–Stokes (RANS) models [35]; Y is the mass fraction of the pollutant distribution; and S is the source term.

2.2.2. Turbulence model

The RANS approach has been adopted in relevant studies to simulate urban airflow fields and pollutant dispersion with successful validation results. The RANS method can also provide reasonable results for mean flows and spatially averaged flow properties in a relatively time-efficient manner. In addition, a sensitivity study of various RANS methods against wind tunnel measurements was conducted, including standard, realizable, re-normalization group (RNG) k-ε turbulence models.

The transport equations for the turbulent kinetic energy (k) and dissipation rate (ε) of a standard k-ε two-equation turbulent model are given by

$$\frac{\partial u_j k}{\partial x_j} = \frac{\partial}{\partial x_j}\left[(\nu + \frac{\nu_t}{\sigma_k})\frac{\partial k}{\partial x_j}\right] + P - \varepsilon \tag{4}$$

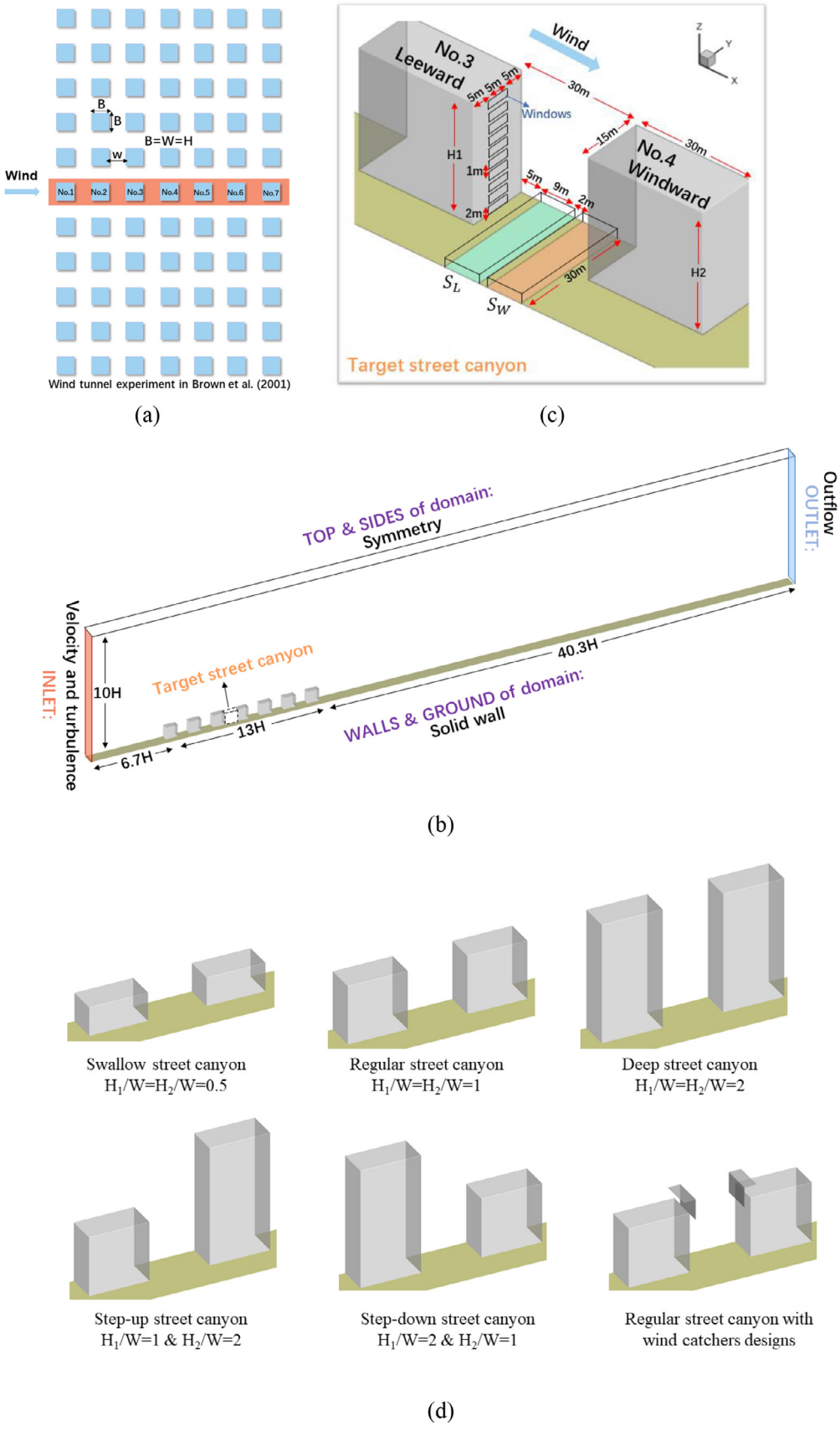

Fig. 2. (a) Model in the wind tunnel test, (b) CFD model description and boundary conditions, (c) setup of the target street canyon, (d) diagrams showing various target street canyon geometries, and (e) CFD grid arrangements of target street canyon for regular street canyon.

$$\frac{\partial u_j \varepsilon}{\partial x_j} = \frac{\partial}{\partial x_j}\left[(\nu + \frac{\nu_t}{\sigma_\varepsilon})\frac{\partial k}{\partial x_j}\right] + C_{\varepsilon 1}\frac{P\varepsilon}{k} - C_{\varepsilon 2}\frac{\varepsilon^2}{k} \quad (5)$$

The production term is defined as

$$P = \nu_t\left(\frac{\partial u_j}{\partial x_i} + \frac{\partial u_i}{\partial x_j}\right)\frac{\partial u_j}{\partial x_i} \quad (6)$$

where μ_t=$C_\mu \rho k^2/\varepsilon$. The constants C_μ, σ_k, σ_ε, $C_{\varepsilon 1}$, and $C_{\varepsilon 2}$, are equal to 0.09, 1.0, 1.3, 1.44, and 1.92, respectively. In parallel, the prediction accuracy of other widespread turbulence models—that is, the realizable and RNG k-ε turbulence models—was further evaluated for comparison.

2.2.3. Case description and boundary conditions

The airflow in the middle column of the aforementioned 3D building arrays is hardly affected by lateral urban boundaries when the lateral width is sufficiently large. To reduce the computational time, only half of the middle column (Fig. 2(b)) was chosen. The full-scale cubic building array ($H = B = W = 30$ m) was numerically investigated at a scale ratio of 1:200 in the CFD simulations. Fig. 2(b) presents the CFD domain and boundary conditions. The computational domain extended from 6.7 H upstream windward face of the first row of cubes to 40.3H downstream leeward face of the last row of cubes, and the distance between the top domain and the ground was 10H. Symmetry boundary conditions are applied on the top and two lateral boundaries of the domain. The outflow boundary condition was set at the domain outlet. The velocity inlet was set at the domain inlet with the vertical profiles of the power-law velocity $U(z)$, turbulent kinetic energy $k(z)$, and its dissipation rate $\varepsilon(z)$.

$$U(z) = U_H \times (z/H)^{0.16} \quad (7)$$

$$k(z) = \frac{(u^*)^2}{\sqrt{C_\mu}} \quad (8)$$

$$\varepsilon(z) = {C_\mu}^{3/4} k^{3/2}/(\kappa_v z) \quad (9)$$

where U_H=3 m/s is the reference inflow velocity under the following conditions: building height $H = 30$ m; $C_\mu = 0.09$, with u^* as the friction velocity (=0.24 m/s); and κ_v as the von Karman constant (=0.41).

Fig. 2(c) describes in detail the target street canyon, which is the secondary street between the No. 3 building and the No. 4 building. Each building consists of 10 floors (each floor with a height of 3 m and window with a height of each 2 m), which are used for further evaluation of air quality index (personal intake fraction, IF_p). Two volumetric CO sources (W_s=9 m, L_y=30 m) are set near the ground with a depth of z = 0–0.5 m to represent the traffic lanes on different sides. The constant emission rates per hour and per unit spanwise street length (36.1 g/h/m, i.e. the total mass release rate, about $L_y \times 1.0 \times 10^{-5}$) are adopted for each CO source, with reference to the study by Ng and Chau [18]. In their calculation of the pollutant release rate, the type and number of vehicles passing a realistic street per hour in Mongkok, Hong Kong were considered. To simulate the non-uniform emission rates induced by TTF, the parameters representing different TTF conditions were set as follows: S_L/S_W=(0.67×10^{-6} kg/m^3/s) / (2.01×10^{-6} kg/m^3/s) =1/3 and S_L/S_W=(2.01×10^{-6} kg/m^3/s)/ (0.67×10^{-6} kg/m^3/s) =3/1, with S_L and S_W as the pollutant source term in leeward and windward traffic lanes, respectively.

The effects of street canyon arrangements on ventilation and pollutant distribution (Fig. 2(d)) were evaluated using five street canyon configurations: shallow street canyon ($H_1/W = H_2/W = 0.5$), regular street canyon ($H_1/W = H_2/W = 1$), deep street canyon ($H_1/W = H_2/W = 2$), step-up street canyon ($H_1/W = 1$ and $H_2/W = 2$), and step-down street canyon ($H_1/W = 2$ and $H_2/W = 1$). H_1 and H_2 denote the upwind building height and downwind building height, respectively. For further pollutant mitigation, two WCs were set near and above the street roof. A WC consists of two perpendicular rectangular walls: a 6 $m \times 12$ m horizontal wall and a 10 $m \times 12$ m vertical wall.

Moreover, three grid arrangements with hexahedral cells and a grid expansion ratio of 1.08 were tested to reduce errors from computational grids for the regular street canyon. Specifically, the minimum grid sizes nearest to the street ground and walls were 0.5 m (coarse grid: 595,626 cells), 0.2 m (medium grid: 1505,028 cells), and 0.1 m (fine grid: 2717,064 cells). By grid independence analysis, the calculated results revealed that satisfactory grid independence could be achieved using the medium grid arrangement (Fig. 2(e)).

2.2.4. Numerical method

The aforesaid governing equations were discretized using the finite volume scheme in the commercial software ANSYS Fluent®. This study used the semi-implicit method pressure-linked equations-consistent or SIMPLEC numerical method for pressure–velocity coupling. The second-order upwind scheme was adopted to discretize both the convective and diffusion terms. A double-precision solver was also selected for CFD calculation. The convergence of the normalized residual errors of the energy equation was set to 10^{-9}, whereas the convergence criterion of the remaining equations was set to 10^{-6}.

3. Results and discussion

3.1. Validation study

Fig. 3 presents a comparison of the CFD predictions by using various k-ε turbulence models (standard, realizable, and RNG k-ε models) and three grid arrangements with wind experiment measurements of the (a) streamwise velocity and (b) turbulence kinetic energy (TKE) at $x/H = 1.5$.

The profiles of the mean streamwise velocity and TKE obtained using the medium-grid were consistent with those obtained using the fine grid. In addition, the difference between the numerical results of the medium grid and the wind-tunnel data was less than that obtained using the coarse grid. Therefore, the medium-grid arrangement was sufficient to achieve grid independence. By using the medium-grid arrangement, various turbulence models were verified. Compared with the other two models, the standard k–ε model (Fig. 3) more efficiently predicted streamwise velocity and particularly, TKE. In the report by Yoshie et al. [41], the modified k-ε models exhibited a lower predictive accuracy than those of the other two models in the simulation of the wake region behind the buildings.

In general, the medium-grid arrangement with the standard k-ε turbulence model could provide the most optimal agreement between the present CFD simulations and wind tunnel measurements.

3.2. Air quality indices

This study uses IF_p as the air quality index, which stands for the fraction of total traffic exhaust inhaled on average by each person in a population, which was first introduced by Hang et al. [42] into CFD simulations to quantify the average personal exposure.

It is defined and calculated as

$$IF\_p = \frac{\sum_i^N \sum_j^M P_i \times Br_{i,j} \times \Delta t_{i,j} \times Ce_j/m}{\sum_j^M P_i} \quad (10)$$

where N is the number of population groups (children, adults, elders, $N = 3$, $i = 1$ to 3), M is the number of different microenvironments (indoors at home, other indoor locations, outdoor locations near vehicles, and other outdoor locations away from vehicles, $M = 4$, $j = 1$ to 4). Only the micro-environment of $j = 1$ (indoor at home) is considered. P_i is the total number of people exposed in the ith population group. $Br_{i,j}$ and $\Delta t_{i,j}$ are the average volumetric breathing rate (m^3/s) and the time spent (s) by individuals in the ith population group in the jth microenvironment, respectively, as summarized by Hang et al. [43]. Ce_j is the pollutant

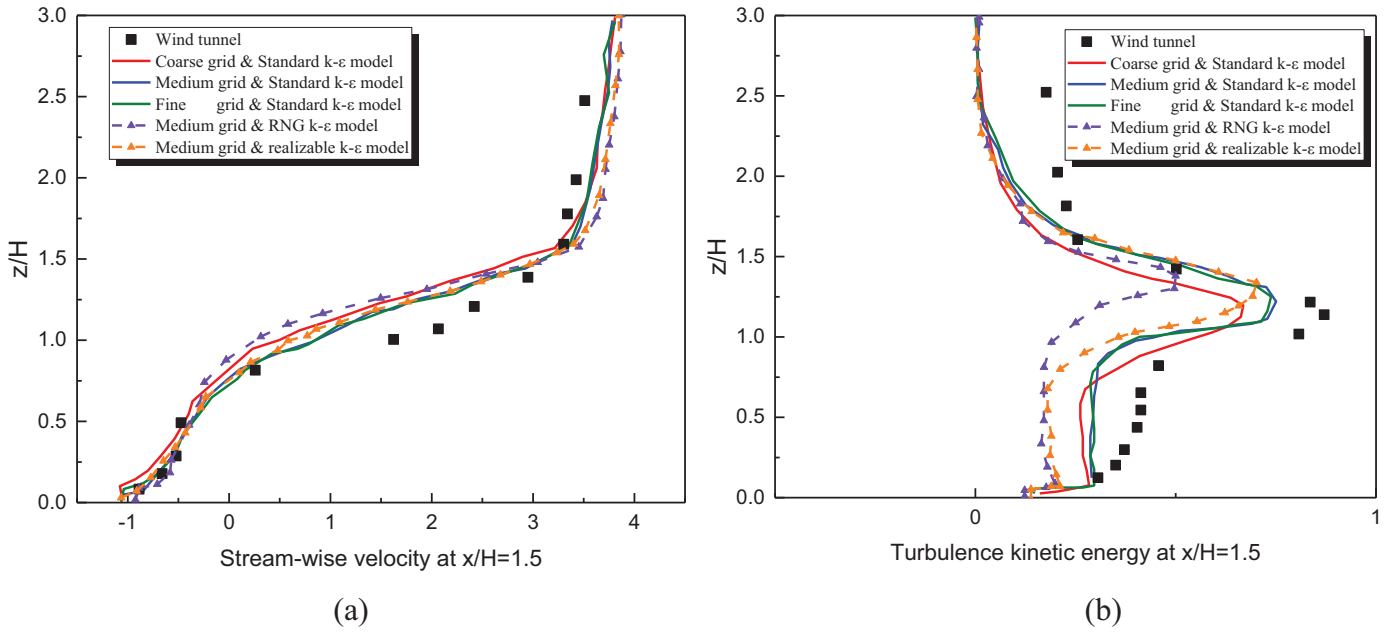

Fig. 3. Comparison of prediction obtained using the wind-tunnel data at x/H = 1.5 on the coarse grid, medium grid, and fine grid with the standard k-ε model, medium with RNG k-ε model, realizable with RNG k-ε model: (a) Streamwise velocity and (b) TKE.

concentration in the *j*th microenvironment (kg/m^3), which can be determined from the area average concentration on the window surface on each floor. *m* is the total emission (kg).

3.3. Effects of street canyon geometry

3.3.1. Effects of street canyon geometry on flow and pollutant dispersion

Fig. 4 illustrates the 3D streamlines, wind velocity, and CO concentration at y/H = 0 in the five street canyons with different geometries (shallow, regular, deep, step-up, and step-down) and different pollutant sources. The geometry of the street canyons significantly affects the flow and the corresponding CO concentration distribution. In the shallow street canyon, only a clockwise vortex appeared; thus the CO concentration is higher in the immediate adjacency of the leeward surfaces, particularly for S_L/S_W = 3/1. The possible reason is that part of CO from windward lanes could disperse upward instead of reaching the leeward surface, but most CO from the leeward lanes flow through the leeward surface before leaving the street canyon. A similar occurrence was observed in the regular street canyon, but the overall concentration was higher than that in the shallow street canyon because of a slightly weaker airflow. Similarly, Hang et al. [43] reported that the CO concentration increased significantly with the depth of the street canyons. In the deep street canyon, the vertically downward airflow mainly comprised the flow structure in the lower space of the street canyon, slightly hindering the dispersion of traffic emission into upper space. Meanwhile, wind velocity near the ground was rather small (about 0.2 m/s). The primary method of pollutant dispersion was molecular diffusion rather than dispersion along streamlines. Consequently, the leeward CO concentration was mainly affected by the leeward lanes, resulting in a higher CO concentration on leeward side was still observed for S_L/S_W = 3/1.

In the step-up street canyon, the high downwind building could introduce more fresh air into the street canyon, significantly increasing the wind velocity. In the lower space of the street canyon, the flow direction near the ground was still from the windward side to the leeward side, hence the higher concentration on the leeward side for S_L/S_W=3/1. In the step-down street canyon, the helical flow with a vertical rotary axis occupied the entire lower space (Fig. 4(e)). Therefore, the difference in concentration between both sides was relatively small despite the higher concentration on the leeward side. Moreover, the concentration distribution was almost identical under different traffic emission configurations.

3.3.2. Effects of street canyon geometry on the concentration of building walls

Fig. 5 shows the CO concentration on the leeward and windward wall surfaces in street canyons with different geometries. First, the maximum concentration on the leeward wall was considerably higher than that on the windward wall in the shallow (0.8 mg/m^3), regular (4.6 mg/m^3), step-up (3.1 mg/m^3), and step-down (3.3 mg/m^3) street canyons, particularly in the lower space (floors 1–4), under different TTF configurations. However, a higher CO concentration was observed on the windward wall in the deep street canyon because the flow near the ground moved from the leeward side to the windward side (Fig. 4(c)). Second, on the leeward wall surfaces, the concentration distribution under different TTF configurations varied completely in the shallow, regular, deep, and step-up street canyons; a higher leeward concentration was obtained when S_L/S_W=3/1. In the step-down street canyon, the leeward concentration distribution was almost identical. On the windward wall surfaces, the concentration distribution was generally similar in the street canyons with different geometries, except that in the deep street canyon. In the deep street canyon, a higher windward concentration was observed when S_L/S_W = 1/3 owing to its main pollutant dispersion mechanism (diffusion) and flow direction near the ground. Third, traffic emission in the street canyons could affect the upper wall on the leeward side, except that in the deep street canyon. In the deep street canyon, only the area from the 1st floor to the 3rd floor was affected by traffic emission under different TTF configurations.

3.3.3. Effects of street canyon geometry on personal intake fraction

Fig. 6 presents the vertical profiles of the CO *IF_p* on different floors in different street canyon geometries. On the leeward side, the *IF_p* from the 1st floor to the 10th floor in the step-down street canyon was considerably higher than those in other street canyons under different TTF configurations, particularly in the lower space (1st floor to 3rd floor). In this regard, the leeward *IF_p* in the step-down street canyon was up to about 1 ppm higher than that in other street canyons. The step-down canyon caused the worst-case scenario and any kinds of TTF can lead to poor air

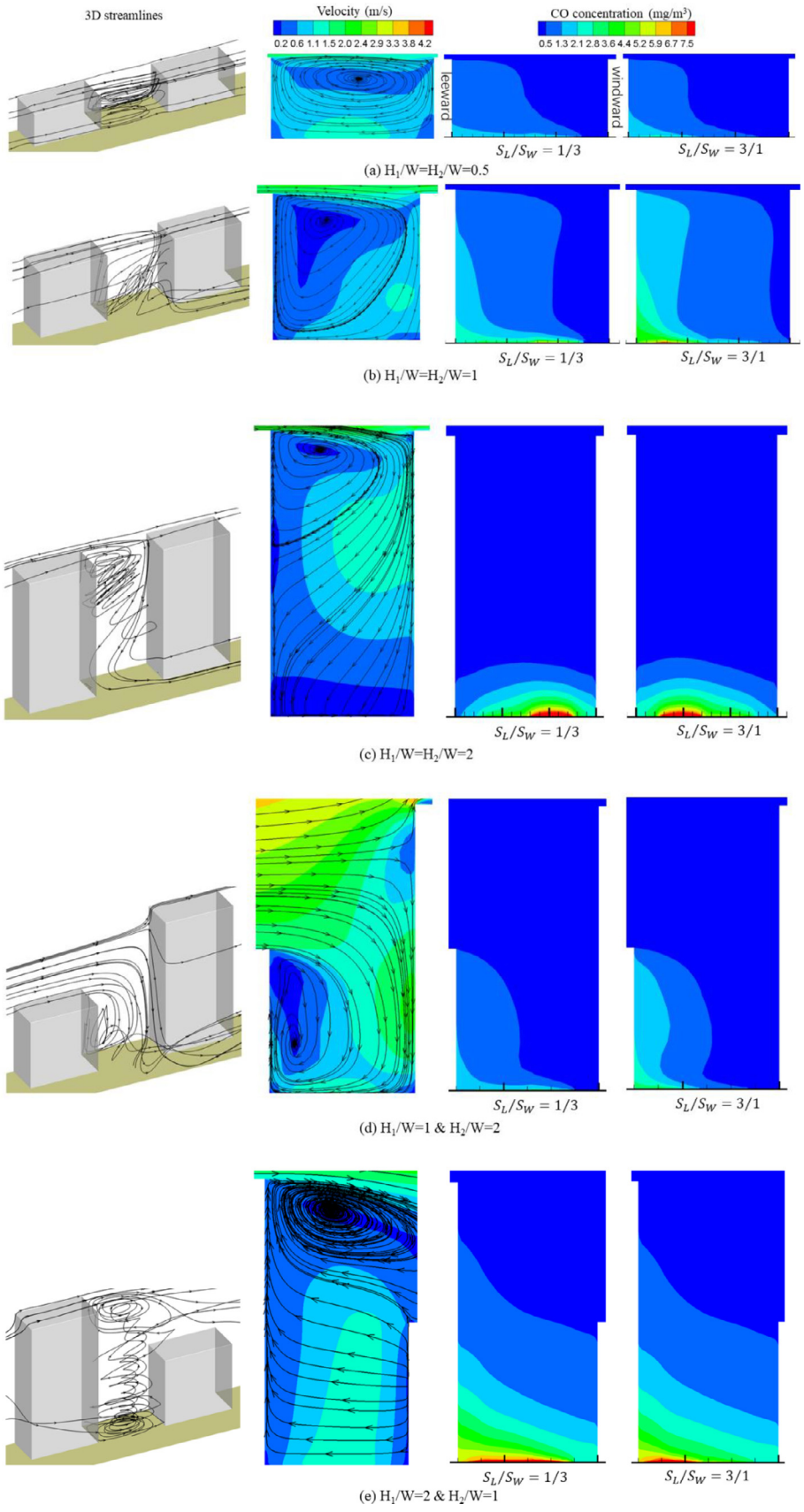

Fig. 4. 3D streamlines, wind velocity, and CO concentration at y = 30 m in (a) the shallow street canyon ($H_1/W = H_2/W = 0.5$), (b) regular street canyon ($H_1/W = H_2/W = 1$), (c) deep street canyon ($H_1/W = H_2/W = 2$), (d) step-up street canyon ($H_1/W = 1$ and $H_2/W = 2$), and (e) step-down street canyon ($H_1/W = 2$ and $H_2/W = 1$).

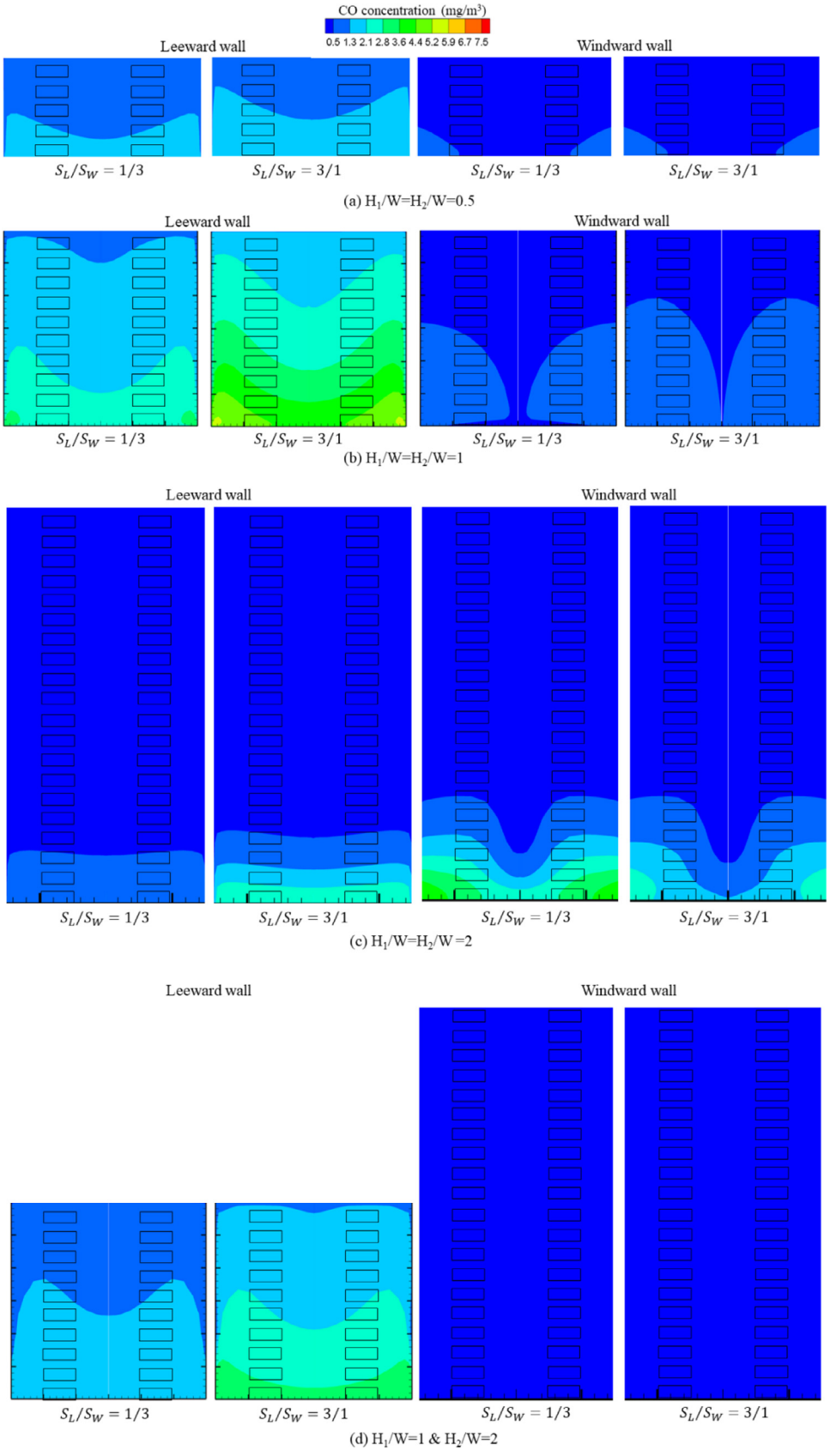

Fig. 5. CO concentration on building walls in street canyons: (a) shallow ($H_1/W = H_2/W = 0.5$), (b) regular ($H_1/W = H_2/W = 1$), (c) deep ($H_1/W = H_2/W = 2$), (d) step-up ($H_1/W = 1$ and $H_2/W = 2$), and (e) step-down ($H_1/W = 2$ and $H_2/W = 1$).

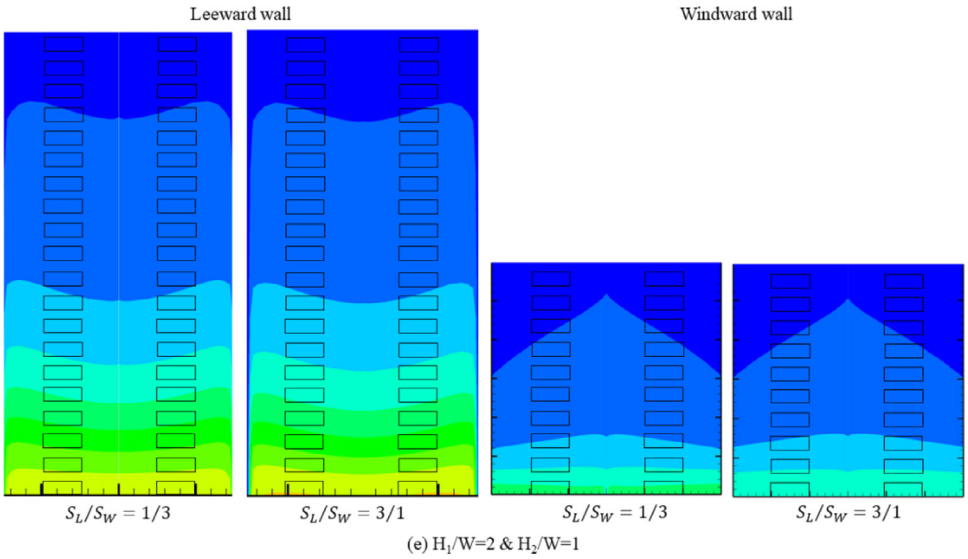

Fig. 5. Continued

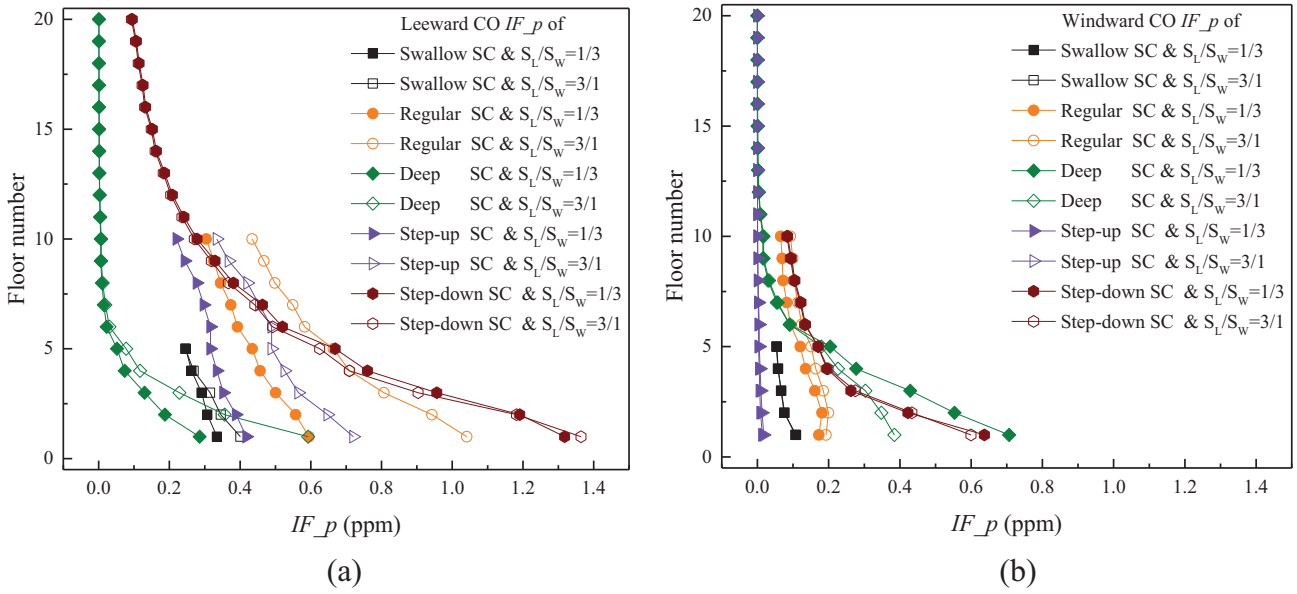

Fig. 6. Vertical profiles of CO *IF_p* in different floors in the street canyons with different geometries.

quality. Subsequently, a relatively higher *IF_p* was observed from the 1st floor to the 10th floor in the step-up and regular street canyons when S_L/S_W = 3/1; the difference in *IF_p* between the different TTF configurations could reach approximately 0.4 ppm. Therefore, the step-up and regular street canyons favored S_L/S_W = 1/3. The leeward *IF_p* was considerably lower in the shallow and deep street canyons than in other street canyons. The windward *IF_p* was substantially higher from the 1st floor to the 5th floor in the deep and step-down canyons than in other street canyons. The largest difference reached approximately 0.7 ppm. Generally, the highest and lowest *IF_p* values under both TTF configurations were observed in the step-down and shallow street canyons, respectively.

3.4. Effects of wind catcher design for various street canyon geometries

3.4.1. Effects of wind catcher design on flow and pollutant dispersion

Fig. 7 presents distinct characteristics (3D streamlines, wind velocity, and CO concentration) relative to the cases without WCs. Altering flow structures within street canyons and increasing wind velocity were effective approaches. In the shallow street canyon with WCs, a clockwise rather than counterclockwise vortex dominated the whole street canyon. In addition, the wind velocity near the leeward side was markedly increased (from 0.4 m/s to about 2 m/s); thus, the leeward CO concentration decreased considerably under different TTF configurations, although the windward CO concentration increased slightly. In the regular street canyon with WCs, the flow structure was completely altered, and the air flow from both sides converged at the center of the street canyon, subsequently flowing from the canopy outward. Therefore, the CO concentration near the surface on both sides decreased significantly under different TTF configurations. In the deep street canyon with WCs, upward and downward helical flows with a vertical rotary axis occupied the upper and lower spaces, respectively. In parallel, the wind velocity near the ground was reinforced, and the pollutant dispersion mechanism changed, facilitating the movement of pollutants. The WCs in the step-up street canyon mainly affected the leeward flow structure. Owing to the WCs, more fresh air was introduced along the leeward surface, further increasing the wind velocity and markedly reducing the leeward CO concentration. In the step-down street canyon with WCs, the flow struc-

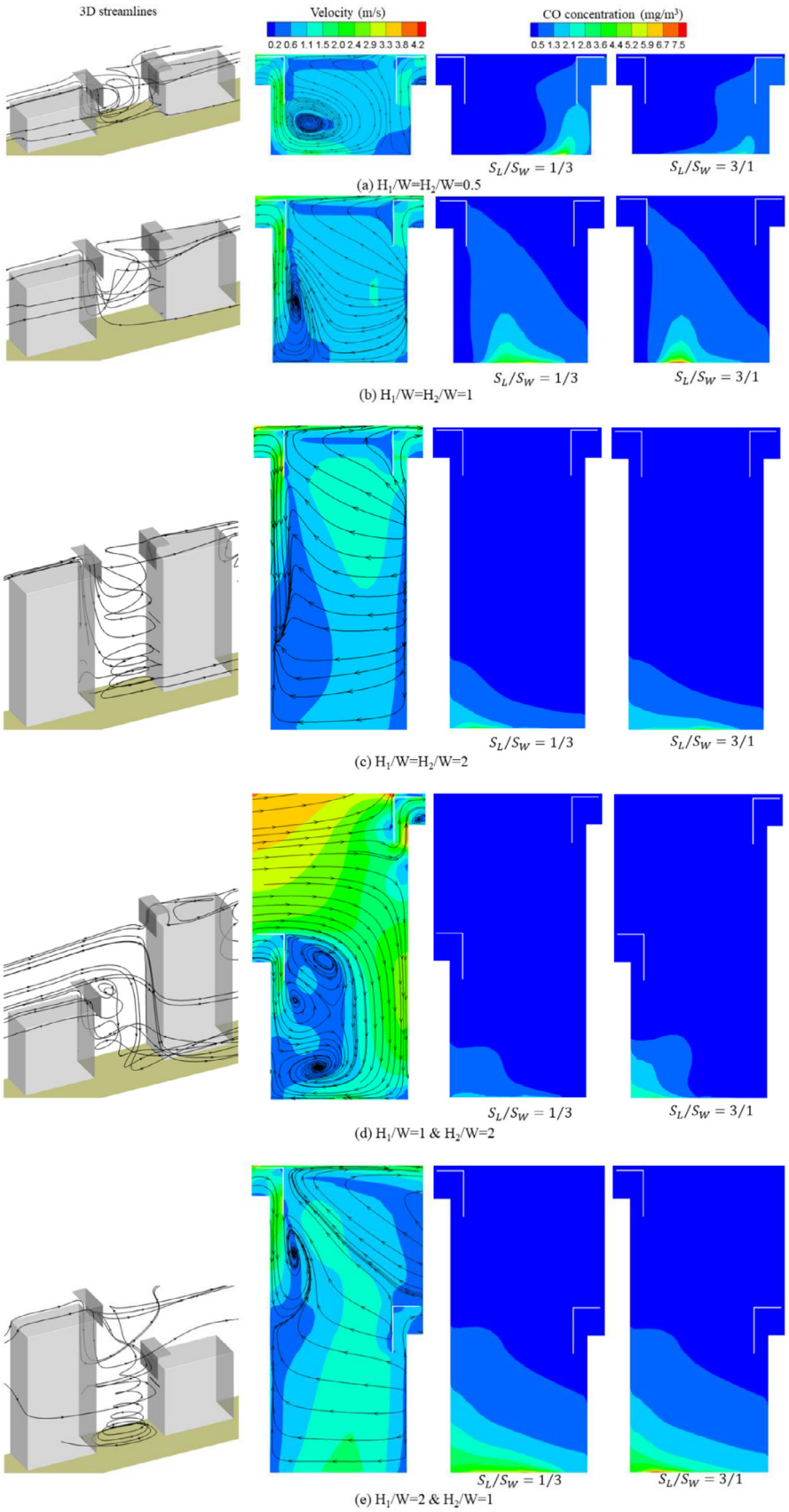

Fig. 7. 3D streamlines, wind velocity, and CO concentration at y = 30 m in the street canyons. (a) Shallow ($H_1/W = H_2/W = 0.5$) and with WC, (b) Regular street canyon ($H_1/W = H_2/W = 1$) with WC, (c) Deep street canyon ($H_1/W = H_2/W = 2$) with WC, (d) Step-up street canyon ($H_1/W = 1$ & $H_2/W = 2$) with WC and (e) Step-down street canyon ($H_1/W = 2$ and $H_2/W = 1$) with WC.

Table 1
Difference in overall average *IF_p* (<*IF_p*>) between cases with WCs and cases without WCs.

Case	Difference in overall average *IF_p* (<*IF_p*>) between cases with WC and cases without WC (%)					
	Leeward			Windward		
	1st–5th floors	5th–10th floors	10th–20th floors	1st–5th floor floors	5th–10th floors	10th–20th floors
Shallow canyon and S_L/S_W = 1/3	99.6	–	–	−8.6		
Shallow canyon and S_L/S_W = 3/1	99.5	–	–	−6.9		
Regular canyon and S_L/S_W = 1/3	91.6	98.7	–	12.8	43.7	
Regular canyon and S_L/S_W = 3/1	94.9	99.2	–	22.9	61.6	
Deep canyon and S_L/S_W = 1/3	−121.7	−258.1	36.7	76.1	56.5	48.3
Deep canyon and S_L/S_W = 3/1	−5.7	−196.1	42.4	59.4	55.3	47.9
Step-up canyon and S_L/S_W =1/3	35.7	99.8	–	46.1	78.4	66.1
Step-up canyon and S_L/S_W = 3/1	30.6	99.8	–	50.9	78.1	65.2
Step-down canyon and S_L/S_W = 1/3	33.8	29.6	88.2	36.7	28.7	–
Step-down canyon and S_L/S_W = 3/1	33.8	30.9	88.4	36.7	29.7	–

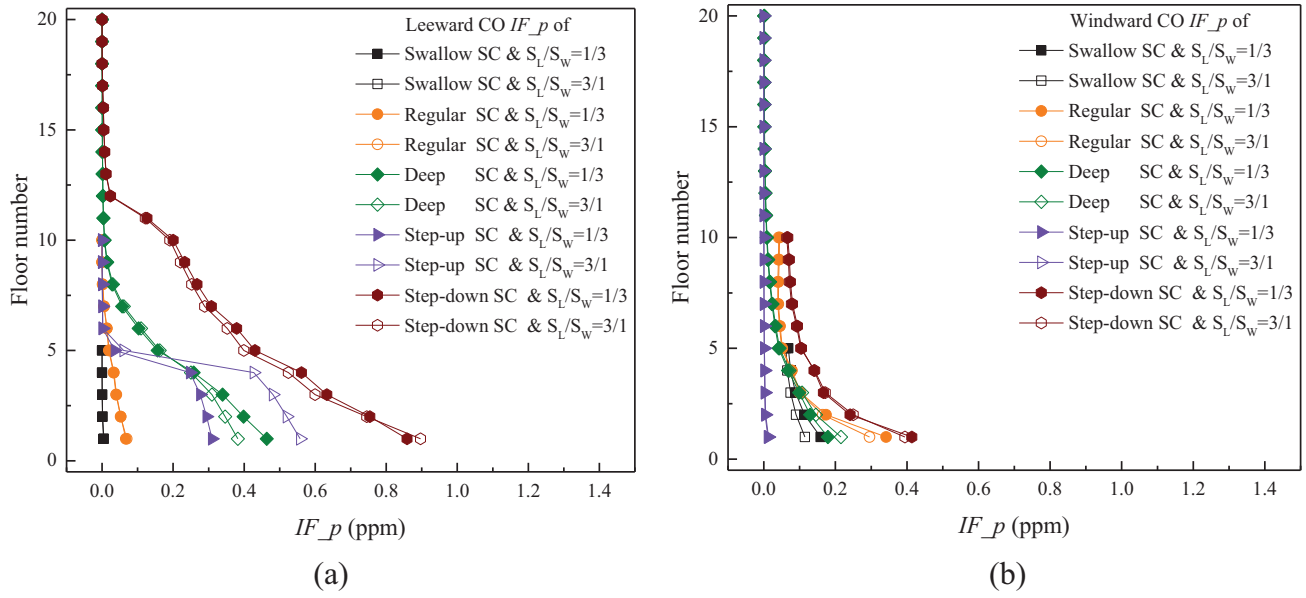

Fig. 8. Vertical profiles of the CO *IF_p* in different floors in the street canyons with different geometries with wind catcher design.

ture in the upper space was noticeably altered, but the upward helical flow dominated the lower space. Consequently, the wind velocity near the ground increased by about 0.3 m/s owing to WCs. CO concentration slightly decreased under the different TTF configurations.

3.4.2. *Effects of wind catcher designs on* IF_p

Fig. 8 presents the vertical profiles of CO *IF_p* in different floors in various street canyon geometries with WCs. Initially, the distribution of the two-side *IF_p* remained nearly the same under different TTF configurations, except for the distribution in the step-up street canyon. In the step-up street canyon, the leeward *IF_p* at S_L/S_W = 3/1 was about 0.3 ppm higher than that at S_L/S_W = 1/3. Second, the *IF_p* could be reduced to different degrees for the different canyon geometries by comparing the *IF_p* in the cases with and without WCs. In the shallow street canyon with WCs, an apparent decline in leeward *IF_p* was observed, and the leeward *IF_p* was close to zero. The windward *IF_p* increased but only slightly. Thus, WCs can help avoid the effects of traffic emission when TTF occurs. Similarly, the leeward *IF_p* decreased significantly, whereas the windward *IF_p* only slightly increased in the regular street canyon with WCs. The WCs could reduce the leeward *IF_p* by as much as 1 ppm. Thus, the WCs can potentially mitigate the air pollution within the regular street canyon under different TTF configurations. In the deep street canyon with WCs, the windward *IF_p* significantly declined, particularly for S_L/S_W=1/3. However, the effects of WCs on leeward *IF_p* was relatively small, and the leeward *IF_p* for S_L/S_W = 1/3 even increased mildly in the lower space. In the step-up street canyon, the WCs could substantially reduce only the leeward *IF_p* above the 4th floor under different TTF configurations. By contrast, WCs largely reduced the two-side *IF_p* below the 5th floor (0.2–0.5 ppm) in the step-down street canyon.

Table 1 compares the overall average *IF_p* (<*IF_p*>) in different floors between the cases with WC and the cases without WC for different street canyon geometries. The WCs could lead to at least 30.6% reduction in the leeward ⟨*IF_p*⟩ for shallow, regular, step-up, and step-down street canyons under different TTF conditions, particularly in the upper space (88.2%–99.6%). However, the leeward ⟨*IF_p*⟩ increased by 258.1% from the 1st floor to the 10th floor but decreased by at least 36.7% from the 10th floor to the 20th floor in the deep street canyon with WCs. WCs could only improve the leeward ⟨*IF_p*⟩ in the upper space of the deep street canyon. A 12.8%–78.4% decrease in windward ⟨*IF_p*⟩ was observed owing to windward WCs in the regular, deep, step-up, and step-down street canyons, whereas a slight increase of about 7% in windward ⟨*IF_p*⟩ was observed in the shallow street canyon. WCs are evidently effective devices for improving the ⟨*IF_p*⟩ on the two sides under different TTF conditions in the shallow, regular, step-up, and step-down street canyons, particularly in the upper space.

4. Conclusion

Increasing traffic emission causes a high risk of exposure for residents in near-road buildings. TTF has gradually become one of the most

important components of urban traffic congestion. Although identical pollutant sources on different sides are usually considered, nonuniform traffic emission under different TTF conditions has rarely been investigated. This study aims to examine the airflow, spatial distribution of pollutants, and *IF_p* of CO in five street canyon structures under different TTF conditions. In addition, an optimal urban design device (WC) is introduced to reduce *IF_p* caused by different TTF conditions in different street canyons. The conclusions are presented below.

The street canyon geometry significantly affects the distribution of *IF_p* in five street canyons under different TTF conditions. Under different non-uniform traffic emission configurations, the maximum leeward *IF_p* was considerably higher than the windward *IF _p* in the shallow (by 0.3 ppm), regular (by 0.9 ppm), step-up (by 0.7 ppm), and step-down (by 0.7 ppm) street canyons; however, a higher maximum *IF_p* was observed on the windward side in the deep street canyon. Moreover, compared with the S_L/S_W = 1/3 TTF condition, the S_L/S_W=3/1 TTF condition led to a higher leeward *IF_p* in the shallow, regular, deep, and step-up street canyons, particularly in the step-up and regular street canyons (the difference in leeward maximum *IF_p* between these two TTF configurations could reach ~0.4 ppm); however, the distribution of the leeward *IF_p* is almost identical for these two TTF conditions in the step-down street canyon. On the windward side, the difference in windward *IF_p* was not significant under different TTF conditions.

The highest (1.4 ppm) and lowest (0.05 ppm) *IF_p* values for any TTF configurations were observed in the step-down and shallow street canyons, respectively. The leeward *IF_p* in the step-down street canyon, from the 1st floor to the 10th floor, was considerably higher than that in other street canyons under different TTF configurations, particularly in the lower space (from the 1st floor to the 3rd floor). The leeward *IF_p* in the step-down street canyon was ~1 ppm higher than the lowest leeward *IF_p* (deep street canyon and S_L/S_W=1/3). On the windward side, the windward *IF_p* from the 1st floor to the 5th floor in the deep and step-down street canyons was substantially higher than those in other cases.

The effects of WCs in the street canyon structures under different TTF conditions vary. The leeward *IF_p* evidently decreased in the shallow and regular street canyons with WCs, and the leeward *IF_p* was almost zero under different TTF conditions. WCs led to a relatively significant decrease in the step-up and step-down street canyons. By contrast, the decrease in windward *IF_p* was relatively slight with WCs. Specifically, WCs could lead to at least 30.6% reduction in leeward overall average *IF_p* (<*IF_p*>) in the shallow, regular, step-up, and step-down street canyons under different TTF conditions, particularly in the upper space (from 88.2% to 99.6%). Similarly, a 12.8%–78.4% decrease in windward ⟨*IF_p*⟩ due to WCs was observed in the regular, deep, step-up, and step-down street canyons.

More attention should be paid to *IF_p* in realistic urban areas in future studies considering realistic TTF conditions. Non-uniform traffic-induced turbulence should also be included in further investigations. This study is one of the first attempts to quantitatively evaluate how *IF_p* is influenced by street canyon geometry under different TTF conditions. This study also adopts an optimal urban design (WCs) to improve air quality caused by TTF, providing practical and meaningful implications for urban planners and designers to solve the air pollution problem.

Conflict of Interest

The authors declare that there is no conflicts of interest.

Acknowledgments

This research was supported by the National Natural Science Foundation of China (Grant No. 51778511), Hubei Provincial Natural Science Foundation of China (Grant No. 2018CFA029), and Key Project of ESI Discipline Development of Wuhan University of Technology (Grant No. 2017001).

References

[1] Z. Li, J. Xu, T. Ming, C. Peng, Numerical simulation on the effect of vehicle movement on pollutant dispersion in urban street, Procedia. Eng. 205 (2017) 2303–2310.
[2] H. Kikumoto, R. Ooka, A numerical study of air pollutant dispersion with bimolecular chemical reactions in an urban street canyon using large-eddy simulation, Atmos. Environ. 54 (2012) 456–464.
[3] Z. Gu, Y. Zhang, Y. Cheng, S. Lee, Effect of uneven building layout on air flow and pollutant dispersion in non-uniform street canyons, Build. Environ. 46 (12) (2011) 2657–2665.
[4] J. Hang, Z. Luo, X. Wang, L. He, B. Wang, W. Zhu, The influence of street layouts and viaduct settings on daily carbon monoxide exposure and intake fraction in idealized urban canyons, Environ. Pollut. 220 (2017) 72–86.
[5] W. Ng, C. Chau, A modeling investigation of the impact of street and building configurations on personal air pollutant exposure in isolated deep urban canyons, Sci. Total Environ. 468 (2014) 429–448.
[6] T.A. Pugh, A.R. MacKenzie, J.D. Whyatt, C.N. Hewitt, Effectiveness of green infrastructure for improvement of air quality in urban street canyons, Environ. Sci. Technol. 46 (14) (2012) 7692–7699.
[7] C. Sha, X. Wang, Y. Lin, Y. Fan, X. Chen, J. Hang, The impact of urban open space and 'lift-up'building design on building intake fraction and daily pollutant exposure in idealized urban model, Sci. Total Environ. 633 (2018) 1314–1328.
[8] B. Blocken, T. Stathopoulos, J. Carmeliet, Application of computational fluid dynamics in building performance simulation for the outdoor environment: an overview, J. Build. Perform. Simu. 4 (2) (2011) 157–184.
[9] P. Cui, Z. Li, W. Tao, Numerical investigations on re-independence for the turbulent flow and pollutant dispersion under the urban boundary layer with some experimental validations, Int. J. Heat Mass Transfer 106 (2017) 422–436.
[10] H. Dou, T. Ming, Z. Li, C. Peng, C. Zhang, X. Fu, Numerical simulation of pollutant dispersion characteristics in a three-dimensional urban traffic system, Atmos. Pollut. Res. 9 (4) (2018) 735–746.
[11] Q. Wang, W. Fang, R. de Richter, C. Peng, T. Ming, Effect of moving vehicles on pollutant dispersion in street canyon by using dynamic mesh updating method, J. Wind. Eng. Ind. Aerod. 187 (2019) 15–25.
[12] H. Huang, R. Ooka, H. Chen, S. Kato, T. Takahashi, T. Watanabe, CFD analysis on traffic-induced air pollutant dispersion under non-isothermal condition in a complex urban area in winter, J. Wind. Eng. Ind. Aerod. 96 (10–11) (2008) 1774–1788.
[13] J. Liu, J. Niu, Delayed detached eddy simulation of pedestrian-level wind around a building array–The potential to save computing resources, Build. Environ. 152 (2019) 28–38.
[14] Y. Du, C.M. Mak, B.S. Tang, Effects of building height and porosity on pedestrian level wind comfort in a high-density urban built environment, Build. Simul. 11 (6) (2018) 1215–1228.
[15] R. De Richter, T. Ming, P. Davies, L. Wei, S. Caillol, Removal of non-CO 2 greenhouse gases by large-scale atmospheric solar photocatalysis, Prog. Energy. Combust. Sci. 60 (2017) 68–96.
[16] Y. He, A. Tablada, N. Wong, Effects of non-uniform and orthogonal breezeway networks on pedestrian ventilation in Singapore's high-density urban environments, Urban Clim. 24 (2018) 460–484.
[17] Y.W. Zhang, Z.L. Gu, Y. Cheng, S.C. Lee, Effect of real-time boundary wind conditions on the air flow and pollutant dispersion in an urban street canyon—large eddy simulations, Atmos. Environ. 45 (20) (2011) 3352–3359.
[18] C. Gromke, B. Ruck, Influence of trees on the dispersion of pollutants in an urban street canyon—Experimental investigation of the flow and concentration field, Atmos. Environ. 41 (16) (2007) 3287–3302.
[19] Z. Tan, J. Dong, Y. Xiao, J. Tu, Numerical simulation of diurnally varying thermal environment in a street canyon under haze-fog conditions, Atmos. Environ. 119 (2015) 95–106.
[20] Z. Tan, J. Dong, Y. Xiao, J. Tu, A numerical study of diurnally varying surface temperature on flow patterns and pollutant dispersion in street canyons, Atmos. Environ. 104 (2015) 217–227.
[21] T. Ming, W. Fang, C. Peng, C. Cai, R. de Richter, M. Ahmadi, Y. Wen, Impacts of traffic tidal flow on pollutant dispersion in a non-uniform urban street canyon, Atmosphere 9 (3) (2018) 82.
[22] F. Ali-Toudert, H. Mayer, Numerical study on the effects of aspect ratio and orientation of an urban street canyon on outdoor thermal comfort in hot and dry climate, Build. Environ. 41 (2) (2006) 94–108.
[23] Z. Baratian-Ghorghi, N.B. Kaye, The effect of canyon aspect ratio on flushing of dense pollutants from an isolated street canyon, Sci. Total Environ. 443 (2013) 112–122.
[24] R.A. Memon, D.Y.C. Leung, C.H. Liu, Effects of building aspect ratio and wind speed on air temperatures in urban-like street canyons, Build. Environ. 45 (1) (2010) 176–188.
[25] Y.H. Juan, A.S. Yang, C.Y. Wen, Y.T. Lee, P.C. Wang, Optimization procedures for enhancement of city breathability using arcade design in a realistic high-rise urban area, Build. Environ. 121 (2017) 247–261.
[26] C.Y. Wen, Y.H. Juan, A.S. Yang, Enhancement of city breathability with half open spaces in ideal urban street canyons, Build. Environ. 112 (2017) 322–336.
[27] J. Gallagher, L.W. Gill, A. Mcnabola, Numerical modelling of the passive control of air pollution in asymmetrical urban street canyons using refined mesh discretization schemes, Build. Environ. 56 (2012) 232–240.
[28] Y.K. Ho, C.H. Liu, S.W. Man, Preliminary study of the parameterisation of street-level ventilation in idealised two-dimensional simulations, Build. Environ. 89 (2015) 345–355.
[29] X.X. Li, C.H. Liu, D. Leung, Numerical investigation of pollutant transport characteristics inside deep urban street canyons, Atmos. Environ. 43 (15) (2009) 2410–2418.

[30] X.X. Li, C.H. Liu, D.Y.C. Leung, K.M. Lam, Recent progress in cfd modelling of wind field and pollutant transport in street canyons, Atmos. Environ. 40 (29) (2006) 5640–5658.
[31] T.R. Oke, Street design and urban canopy layer climate, Energy Build. 11 (1–3) (1988) 103–113.
[32] S. Vardoulakis, B.E.A. Fisher, K. Pericleous, N. Gonzalez-Flesca, Modelling air quality in street canyons: a review, Atmos. Environ. 37 (2) (2003) 155–182.
[33] X. Xie, Z. Huang, J. Wang, The impact of urban street layout on local atmospheric environment, Build. Environ. 41 (10) (2006) 1352–1363.
[34] C.H. Liu, W.C. Cheng, T.C.Y. Leung, D.Y.C. Leung, On the mechanism of air pollutant re-entrainment in two-dimensional idealized street canyons, Atmos. Environ. 45 (27) (2011) 4763–4769.
[35] F. Murena, G. Favale, Continuous monitoring of carbon monoxide in a deep street canyon, Atmos. Environ. 41 (12) (2007) 2620–2629.
[36] J. Boddy, R. Smalley, N. Dixon, J. Tate, A. Tomlin, The spatial variability in concentrations of a traffic-related pollutant in two street canyons in york, UK—Part I: the influence of background winds, Atmos. Environ. 39 (17) (2005) 3147–3161.
[37] J.J. Baik, R.S. Park, H.Y. Chun, J.J. Kim, A laboratory model of urban street-canyon flows, J. Appl. Meteorol. 39 (9) (2000) 1592–1600.
[38] M.A. Nelson, E.R. Pardyjak, J.C. Klewicki, S.U. Pol, M.J. Brown, Properties of the wind field within the oklahoma city park avenue street canyon. part I: mean flow and turbulence statistics, J. Appl. Meteorol. Climatol. 46 (12) (2015) 2038–2054.
[39] L. Chew, N. Nazarian, L. Norford, Pedestrian-level urban wind flow enhancement with wind catchers, Atmosphere 8 (9) (2017) 159.
[40] K. Zhang, G. Chen, X. Wang, S. Liu, C.M. Mak, Y. Fan, J. Hang, Numerical evaluations of urban design technique to reduce vehicular personal intake fraction in deep street canyons, Sci. Total Environ. 653 (2019) 968–994.
[41] R. Yoshie, A. Mochida, Y. Tominaga, et al., Cooperative project for CFD prediction of pedestrian wind environment in the Architectural Institute of Japan, J. Wind. Eng. Ind. Aerod. 95 (9–11) (2007) 1551–1578.
[42] J. Hang, Z. Luo, X. Wang, L. He, B. Wang, The influence of street layouts and viaduct settings on daily carbon monoxide exposure and intake fraction in idealized urban canyons, Environ. Pollut. 220 (2017) 72–86.
[43] J. Hang, Z. Xian, D. Wang, C.M. Mak, B. Wang, Y. Fan, The impacts of viaduct settings and street aspect ratios on personal intake fraction in three-dimensional urban-like geometries, Build. Environ. 143 (2018) 138–162.